Fabrication, morphology and thermal properties of alkylated graphene oxide-modified phase-change microcapsules for thermal energy storage

Da-Zhu Chen[1,*], Si-Yin Qin[1], Gary C. P. Tsui[2],Chak-yin Tang[2], Xing Ouyang[1], Jia-Hua Liu[1], Jiao-Ning Tang[1], Jian-Dong Zuo[1]

[1] *Shenzhen Key Laboratory of Polymer Science and Technology, College of Materials Science and Engineering, Shenzhen University, Shenzhen 518060, China*

[2] *Department of Industrial and Systems Engineering, The Hong Kong Polytechnic University, Hung Hom, Kowloon, Hong Kong, China*

[*] *Corresponding author: E-mail: dzchen@szu.edu.cn; Tel: (+86)755 8671 3934; Fax: (+86)755 2653 4457*

Abstract

The demands for achieving microencapsulated phase-change materials (MEPCMs) with high thermal-energy storage ability have motivated increasing research interest in inorganic filler-modified MEPCMs. However, challenges for such MEPCMs still exist in the pursuit of good compatibility of inorganic particles with the core or shell material. Here, a novel type of octadecylamine-grafted graphene oxide (GO-ODA) -modified MEPCMs using melamine-formaldehyde (MF) resin as the shell material and the mixture of GO-ODA and *n*-octadecane as the core material was fabricated via in-situ polymerization. The alkylated GO with a thickness of ~ 1 nm was confirmed to be highly compatible with the core material. The as-prepared MEPCMs with a regular spherical shape were dispersed without any agglomeration, and the size decreased with increasing the filling amounts of GO-ODA. The incorporation of GO-ODA promoted the crystallization of *n*-octadecane, resulting in an observable reduction in supercooling

degree. The encapsulation efficiency of MEPCMs was calculated to be over 88.0%, and the melting/freezing latent heats reached to a level as high as 207.2 J g^{-1} and 202.5 J g^{-1}, respectively, even at a tiny loading level of 0.5 %. Besides, the GO-ODA incorporated MEPCMs showed a good thermal cycling stability during a phase change. Moreover, a substantial enhancement in thermal transfer rate? and a less marked heating effect for the MEPCMs containing GO-ODA were observed from the thermal conductivity tests and infrared thermography analysis. The findings suggested that the prepared MEPCMs are promising for applications in the fields of thermal energy storage and temperature regulation due to their enhanced thermal transfer performance and prominent phase-change enthalpy.

Keywords: Microencapsulated phase-change materials; Graphene; Thermal properties; Thermal energy storage

1. Introduction

Microencapsulated phase-change materials (MEPCMs) have attracted increasing research interest during the past few decades because of their good application potential in the fields of thermal energy storage and temperature regulation. The melting and crystallization processes of the core material and the resulting absorption/release of amounts of latent heat take place in the microcapsule within a quite narrow temperature scope [1]. Due to the protection of organic/inorganic shell, the leakage of the melted PCMs is suppressed, the heat-transfer ability is improved, and the reactivity of PCMs with the outside environment is reduced [2-4]. So far, the applications of MEPCMs for smart building materials [3], thermal protection of electronic devices [5], waste heat utilization [6] and temperature-adjustable textiles [7,8] or biodegradable polymer films [9], etc., have been widely investigated, especially for the areas where high latent heat

and prompt thermal-response ability are particularly pursued.

Compared to inorganic or solid-solid PCMs, solid-liquid organic PCMs, including paraffin waxes, fatty alcohols, fatty acids and their derivatives, possess superior properties, such as high latent heat, non-toxicity and anti-corrosive property, limited volume change, and good stability [10,11], and thus have been widely used for fabricating MEPCMs. In order to achieve good mechanical performances, low supercooling extent and prompt response to minute changes in the ambient temperature, various inorganic fillers were incorporated into the core or shell structure of MEPCMs. For example, Jiang et al. [12] prepared the nano-Al_2O_3-filled microcapsules with a paraffin wax core and a poly (methyl methacrylate-co-methyl acrylate) shell, and found that the MEPCMs, after incorporation of 16 wt % nano-Al_2O_3 of monomer, achieved 93.41 J g^{-1} in enthalpy and 0.31 W m^{-1} K^{-1} in thermal conductivity. Li et al. [13] synthesized the MicroPCMs with urea-formaldehyde resin as the shell and the mixture of paraffin and stearyl alcohol-grafted carbon nanotubes (CNTs) as the core material, and an increase of 79.2 % in thermal conductivity was found after the incorporation of 4.0 % CNTs. More recently, the authors [14] involved the vermicular multi-walled CNTs into the walls of MEPCMs via a layer-by-layer self-assembly method, and found that both the mechanical properties and thermal transportation of the MEPCMs were greatly improved with increasing the content of assembled CNTs.

Among inorganic fillers, graphene has become an attractive material for modifying microcapsules owing to its outstanding electrical, thermal, and mechanical properties [15-17]. Chen et al. [18] reported that the MEPCMs with an melamine-formaldehyde (MF) resin/graphene oxide (GO) composite shell displayed an increase of 66.29 % in thermal conductivity, when 4 wt% of GO was involved, compared to that of bare MEPCMs. Yuan et al. [19] prepared the phase-change slurry containing MEPCMs of

paraffin@SiO_2/GO, and found that both the thermal conductivity and the heat-storage capacity along with the remarkable photo-thermal conversion performance were enhanced, because of the incorporation of GO [19]. However, till now, almost all the literatures on graphene-modifying MEPCMs reported that the water-soluble GO nano-sheets were incompatible with the organic PCMs, and thus could not achieve the stable dispersion within the core of MEPCMs. On the other hand, inorganic fillers have higher density than that of core and shell materials of MEPCMs, and thus the improvements in thermal conductivity and mechanical performances due to the introduction of inorganic fillers will sacrifice a certain amount of latent heat, resulting in a noteworthy reduction in energy storage capability. The challenge is how to improve the dispersion of micro-/nano-particles within MEPCMs so as to mitigate the negative influence by decreasing their content to a low level. In this work, we present, for the first time, the experimental investigation of an oil-soluble alkylated graphene (GO-ODA)-modified MEPCMs using MF resin as the shell material and the mixture of GO-ODA and *n*-octadecane as the core material. The GO-ODA with the thickness of ~ 1 nm, prepared through the first oxidation and thereafter grafting with octadecylamine, was verified to be highly compatible with the core material. The GO-ODA-modified MEPCMs exhibited substantial enhancement in thermal conductivity and energy storage ability, even at very tiny loading level.

2. Experimental

2.1. Materials

n-Octadecane (99 %), melamine (98 % purity), fomaldehyde solution (AR，37 %), octadecylamine (90%), thionyl chloride (AR, 99%) were purchased from the Aladdin Chemistry Company Ltd (China). Styrene-maleic anhydride copolymer (SMA, AR)

supplied by the Beijing THK Sci. Co., Ltd was used as the emulsifier after being treated with NaOH at 90 °C for 3 hours to form a 10 wt% sodium salt solution. $KMnO_4$ (99%), and H_2SO_4 (98%) was provided by the Shanghai Chemical Reagent Co. $NaNO_3$ (AR) and N,N-dimethylformadide (DMF,AR) were obtained from the Tianjin Chemical Reagent Factory. Nano-graphene platelets (NGPs) with a diameter of 5-10 μm, a thickness of 4-20 nm and a purity of higher than 99.5 wt% were purchased from the Chengdu Organic Chemicals Company Ltd. The layer number of NGPs was less than 20.

2.2. Preparation of GO and GO-ODA

The preparation of GO was performed using a modified Hummers method [18,20] from NGPs. Briefly, NGPs (4 g) and 92 ml of concentrated sulfuric acid (98 wt%) were mixed in a 500 ml three-neck flask under an ice bath, followed by adding 1 g of sodium nitrate. After 30 min of stirring at 400 rpm, 12 g of potassium permanganate was slowly added and continuously stirred for 2 h to exfoliate the mutilayer graphene to a single layer one (Fig. 1). Then, the suspended system was stirred at 35 °C for 30 min. Thereafter, 184 ml of distilled water was slowly added into the flask, meanwhile, the reaction temperature was raised to 98 °C and maintained for 15 min. Next, H_2O_2 (30%, 30 ml) was added to reduce the residual oxidant. Finally, the resulting suspension was centrifuged and washed with warm distilled water several times until the solution became neutral. After 24 h of vacuum freeze-drying, the dried oxygen-rich GO powders were obtained. The hydrogen content and a mole ratio of C/H of the as-prepared GO powders were determined to be 2.10±0.01wt% and 22.63±0.16%, respectively, using a vario EL cube elemental analyzer.

The alkylation of GO includes two steps: activation of carboxylic groups on the edge

of GO nanosheets and subsequent graft process using octadecylamine (ODA) [21,22]. First, GO (2g), $SOCl_2$ (400 ml) and DMF (4 ml) were mixed in 500ml three-neck round-bottomed flask in an ice bath via 1 h of ultrasonication with the power of 300 W. The formed homogeneous suspension solution was then refluxed at 70 °C for 24 h using a condenser equipped with a $CaCl_2$-filling guard tube. After being cooled down to atmosphere temperature, the resulting solution was filtrated and rinsed with ample amount of CH_2Cl_2 several times to remove excess $SOCl_2$, followed by vacuum drying at 50 °C for 12 hours. Second, to graft the octadecyl chain onto the GO nanosheets, the above activated GO was allowed to react with ODA at 120 °C for 4 days. Afterward, the reaction mixture was filtrated and washed with excess hot ethanol several times. The shiny black filter cake of GO-ODA was finally dried at 50 °C in a vacuum oven for 12 h.

2.3.1 Fabrication of MEPCMs with and without GO-ODA

The fabrication process of MEPCMs with the GO-ODA is illustrated in Fig. 2. The proportions of the used materials including *n*-octadecane and GO-ODA are listed in Table 1. First of all, 6.0 g of melamine, 11 g of 37 % formaldehyde aqueous solution, and 10 ml of distilled water were added to a 250 ml three-neck round-bottomed flask, and kept reacting at 70 °C and pH 9.0 for 1 h to form the melamine-formaldehyde (MF) resin prepolymer. Meanwhile, certain amounts of GO-ODA and *n*-octadecane were homogenously mixed via ultrasonic dispersion at 70 °C water bath for 30 min. Then, the mixture was poured into 3 % SMA solution and vigorously stirred at the same temperature for 50 min with an agitation speed of 1800 rpm to form a stable oil-in-water (O/W) emulsion. Next, the above prepared MF-prepolymer was added dropwise into the emulsion to initiate the formation of MF shell on the microcapsules. The

polymerization and crosslinking of prepolymers were conducted at a pH value of 4.5 for 3 h. The GO-ODA-doped MEPCM powders were achieved by fully washing and subsequent vacuum freeze-drying. As shown in Table 1, the amounts of GO-ODA were controlled to be 0.1 %, 0.2 %, and 0.5 % in relation with that of *n*-octadecane, and the corresponding microcapsules were nomenclated as MEPCM-01, MEPCM-02, and MEPCM-05, respectively. For comparison, the bare MEPCMs, named as MEPCM-00, were also fabricated using the similar procedure without the addition of GO-ODA.

3. Characterization

Fourier transform infrared (FTIR) spectra of the GO-ODA and MEPCMs were measured using a PerkinElmer FTIR spectrometer in the range of 4000-600 cm^{-1} using the KBr sampling method. Raman spectra were obtained using a Renidhaw invia Raman spectrometer operated at room temperature with an argon-ion laser resourse and a back-scattering geometry with an excitation wavelength of 514.5 nm.

The size and thickness of the GO and GO-ODA nanosheets were characterized using a Bruken Dimension Icon atomic force microscope (AFM) in the tapping mode. The samples for observation were prepared by depositing the dispersions of GO and GO-ODA on a cleaved mica surface. The morphologies of MEPCMs were observed using a Hitachi Su-70 field emission-scanning electron microscope (FE-SEM) at an accelerating voltage of 5.0 kV. The size distributions of microcapsules were tested by a BT-9300ST laser particle size analyzer using deionized water as the dispersion medium. An Mshot MP41 optical microscope (OM) equipped with a MC 50 digital imaging system (Guangzhou Micro-shot Technology Co., Ltd., China) was used to observe the formation of the microcapsules.

X-ray diffraction (XRD) patterns were recorded on an X-ray diffractometer (Bruker

D8 ADVANCE Germany) with Cu Kα radiation (λ = 0.154 nm) at 40 kV, 200 mA. The step size is 0.02 º.

The phase-change properties of *n*-octadecane and MEPCMs were analysed utilizing a TA Q200 differential scanning calorimeter (DSC). About 5 mg of powders were used for each test cycle at a heating/cooling rate of 5 °C/min and a temperature range of 0 to 50 °C under the nitrogen atmosphere protection.

The measurement of thermal conductivity of MEPCMs was conducted using a hot disk thermal constant analyzer (TPS 2500S, Sweden) with the C7577 probe at room temperature. For the repeatability of the results, at least five measurements were performed for each sample.

The thermal-regulating properties of MEPCMs filled with GO-ODA were assessed using an infrared thermal imager (Fluke TiS65). Prior to the tests, 20 wt% of MEPCMs were incorporated into epoxy resin and hardened in a cylindrical mold to form round composite disks with a diameter 15 mm and a thickness of 3.4 mm. As a control, a raw epoxy resin disk was also fabricated with the same size. All disks were cooled to 0 °C beforehand, and placed onto a hot stage maintaining at 60 °C during the test. A 5 mm-thick cylindrical polytetrafluoroethylene (PTFE) disc with a diameter of 15 mm was placed between the hot plate and the test sample to prevent the disk temperature from rising too quickly. The lens of microscope was kept at 25 cm from the upper surface of the disk. The infrared thermal images were taken at different times until the temperature rose up to 50 ℃, and analyzed using the SmartView 4.3 software.

3. Results and discussion

3.1. Structure of GO and GO-ODA

Figure 3 shows the FTIR spectra of GO-ODA, ODA and GO. The FTIR spectrum of

GO includes the typical absorption peaks of oxygen-containing groups: O-H stretching vibration (3400 cm^{-1}), C=O stretching vibration in carboxylic acid and carbonyl moieties (1733 cm^{-1}), C-OH stretching vibration (1437 cm^{-1}), C-O-C stretching vibration (1258 cm^{-1}), C-O stretching vibration (1062 cm^{-1}) [23,24]. After being modified with ODA, the GO became GO-ODA and the spectrum illustrates the presence of C-H stretching vibration on the methylene and methyl of alkyl groups (2917, 2846 cm^{-1}), C=O stretching vibration of the amide (1656 cm^{-1}) [25], the overlapped signature of the N-H and sp^2 carbon dominates? (1564 cm^{-1}) [26], the stretching mode of C-N linkage of amide (1189 cm^{-1}) [27] and C=O stretching vibration of carboxylic groups (1733 cm^{-1}). The occurrence of these peaks on GO-ODA spectrum means that ODA has been grafted on GO successfully. The inset of Fig. 3 compares the dispersions of GO-ODA in melted *n*-octadecane and deionized water. It can be revealed that the graphene oxide has become highly hydrophobic after the graft of octadecyl chain, indicative of a good dispersion stability of GO-ODA in the core of *n*-octadecane of MEPCMs when undergoing melting/freezing cycles during the use.

The AFM images of as-prepared GO and GO-ODA are presented in Figs. 4a and b. The size of the GO nano-platelets is mainly distributed in the range between 0.7 μm and 1.6 μm, and becomes smaller after alkylation after one hour of ultrasonication as mentioned above. As shown in Figs. 4c and d, the GO and GO-ODA platelets exhibit the same thickness of ~1 nm, indicating that a complete exfoliation of multi-layered graphene was achieved.

3.2. Structure and morphologies of MEPCMs with and without GO-ODA

Figure 5 shows the images of as-prepared microcapsules with and without graphene. It can be seen that the MEPCMs without GO-ODA are loose white powders; however,

when GO-ODA is involved in the microcapsules, the color becomes grey. The geometric profiles of MEPCM powders with various amounts of GO-ODA are displayed in the SEM images (Figs. 6a-e). The microcapsules are spherical and well dispersed without any agglomeration. The shell thickness of MEPCMs is approximately 320 nm (Fig. 6e). Interestingly, when comparing the size of microcapsules filled and unfilled with GO-ODA, it can be easily found that the introduction of GO-ODA tends to decrease the dimension of phase-change microcapsules. This changing trend of microcapsule size can also be reflected in the size distribution measured using the laser particle size analyzer (Fig. 6f). The most size fraction for bare MEPCMs is about 24.69 μm, while for MEPCMs filled with 0.1 %, 0.2 %, and 0.5 %, it has become 16.09 μm, 14.46 μm and 11.68 μm, respectively. It is anticipated that, when hydrophilic GO were grafted with long alkyl chains (Fig. 1), the graphene nano-platelets were endowed with a hydrophilic-lipophilic structure, similar to that of traditional emulsifier, and thus during the emulsion of the core material within the SMA solution, the alkylated GO would function as a co-emulsifier, stabilize the oily emulsion droplets, and minimise the re-combination between adjacent droplets, resulting in the formation of smaller microcapsules.

Figure 7 shows the FTIR spectra of GO-ODA, MF resin, *n*-octadecane, and MEPCMs with and without GO-ODA. In the spectrum of MF resin, the broad absoption band at ~3400 cm^{-1} is assigened to the superposition of O-H and N-H stretching vibrations. The C-O-C stretching vibrations are located at 1163 cm^{-1}. Similar absorption peaks are observed in the spectra of MEPCMs with and without GO-ODA. The strong peaks at 2925 cm^{-1} and 2853 cm^{-1} are attributed to the aliphatic C-H streching vibrations of $–CH_2$ and $–CH_3$, respectively. The peaks at 1467 cm^{-1} and 721 cm^{-1} are associated with the in-plane bending vibration peaks of $–CH_2$, which can be observed in the spectra

of *n*-octadecane and microcapsules, but are invisible for the MF shell due to the less –CH_2 in the chemical structure of MF resin [28]. The peak at 721 cm^{-1} is considered to be the characteristic peak of alkyl $(CH_2)_n$ ($n \geqslant 4$). In-plane and out-of-plane triazine ring vibrations appear at 1557 cm^{-1} and 811 cm^{-1}, respectively [29]. In addition, the characteristic absoption peaks of multiple C-N streching for the triazine ring at approximately 1557 cm^{-1} and 1488 cm^{-1} are found in either MF resin, or MEPCM-00 and MEPCM-01, which confirms that the *n*-octadecane had been encapsulated with MF resin through the in-situ copolymerization process [18,28]. Owing to the tiny loading level in microcapsules, nearly no characteristic peaks for graphene can be observed from the spectrum of GO-ODA-filled microcapsules. However, the existance of GO-ODA in microcapsule can be verified in the Raman spectra of GO-ODA and MEPCMs (Fig. 8). Generally, referring to the Raman spectroscopy of carbonaceous materials, e.g., carbon and its compounds, there typically exist the broad D-band and G-band [17,30-32]. The former is related to vibrations of carbon atoms with dangling bonds in plane terminations of graphene and associated with the lattice damage of graphene and amorphous carbon [33], while the latter is attributed to the vibration of sp^2-bonded carbon atoms in a 2D hexagonal lattice, acting as decisive roles on properties of graphene. In Fig. 8, other than that of bare MEPCMs, the D-peak at 1348 cm^{-1} and G-peak at 1578 cm^{-1} for GO-ODA can be clearly observed in the spectra of MEPCMs filled with various amounts of GO-ODA, which reveals the incorporation of graphene within the microcapsules.

Figure 9 shows the XRD patterns of GO-ODA, MF, *n*-octadecane, MEPCM-00 and MEPCM-01. The GO-ODA shows a broad diffraction peak between 20^o and 28^o due to the poor crystallinity of alkylated graphene [21]. The amorphous diffraction peak of MF resin was observed nearly at the same position. The sharp diffraction peaks at 2θ

of 19.25°, 19.75°, 23.36° and 24.76° are assigned to (005), (011), (102) and (-111) reflections of the α-crystal phase of *n*-octadecane, respectively. The β-crystal reflections of *n*-octadecane are related to the peaks at $2\theta = 7.76°$, 11.49° and 15.38°, corresponding to (002), (003) and (004) planes. All the characteristic diffraction peaks of *n*-octadecane appear in the XRD spectra of both MEPCM-00 and MEPCM-01, indicating the encapsulation of *n*-octadecane within the microcapsules.

3.3. Phase-change behaviors

The phase-change behaviors of *n*-octadecane and MEPCMs containing various amounts of GO-ODA were investigated by DSC, and the resulting thermograms are presented in Fig.10. The melting and crystallization properties of all the samples are listed in Table 2. During the heating process, the onset melting temperature ($T_{m,s}$) and the peak temperature (T_m) of microcapsules with and without GO-ODA are close to those of *n*-octadecane. After encapsulation, the melting peak of *n*-octadecane becomes broader, and a rise of 3.44 - 4.22 °C in the melting width ($\triangle T_{m,w}$), i.e., the difference of the onset temperature and the end temperature ($T_{m,e}$) was examined. In the cooling process, the *n*-octadecane shows a sole sharp crystallization peak at 25.17 °C with an onset temperature ($T_{f,s}$) of 26.20 °C corresponding to the homogeneous nucleation of β-crystallization [34]. After microencapsulation with MF resin, the crystallization peak of *n*-octadecane becomes wider, and besides the β-crystallization peak, there appear two other visible exothermic shoulder peaks, namely α- and γ-peaks, corresponding to the heterogeneously nucleated liquid-rotator transition and the homogeneously nucleated rotator-crystal transition, respectively [35]. Compared to the bare MEPCMs, the microcapsules with various amounts of GO-ODA display the increases of 3.53 °C

in $T_{f,s}$, 5.89 °C in T_{α}, 5.38 °C in T_{β}, and 3.17 °C in T_{γ}, respectively. This means that the incorporation of the alkylated graphene within the microcapsules had advanced the crystallization of core material to some degree because of the enhanced heterogeneous nucleation and thermal transfer by the GO-ODA nano-platelets, and as a result, the supercooling of core material was suppressed. The enthalpies of melting and freezing ($\triangle H_m$ and $\triangle H_f$) for *n*-octadecane are 233.1 J g^{-1} and 232.5 J g^{-1}, respectively. After encapsulation, the values of $\triangle H_m$ and $\triangle H_f$ decrease, but still maintain a high level larger than 207.2 J g^{-1} and 202.5 J g^{-1}, respectively, even if the amount of GO-ODA increases to 0.5 %. The encapsulation efficiency (*E*) of MEPCMs was calculated to be more than 88.0 % according to the equation [36] $E = (\triangle H_{m,MEPCMs} + \triangle H_{f,MEPCMs})/(\triangle H_{m,PCM} + \triangle H_{f,PCM}) \times 100\%$. Apparently, the high phase-change latent heat and encapsulation efficiency of the prepared MEPCMs, as well as the mild phase-change temperature will benefit their practical application as micro-vehicles for energy storage and temperature regulation.

3.4. Thermal reliabilities of microcapsules

Figure 11 shows the DSC curves of MEPCMs after 30 heating-cooling cycles. The thermal cycling curves between 0 °C and 50 °C with the interval of 10 cycles are nearly completely coincidental, either for the bare MEPCMs or for the MEPCMs filled with GO-ODA. Correspondingly, the phase-change temperature and the latent heat of MEPCMs with and without GO-ODA exhibit nearly no changes from the first cycle to the 10th, 20th and 30th cycles, which is indicative of the outstanding thermal cycling stability during the phase change.

3.5. Evaluation of the thermal-regulated properties

The thermal conductivity is a vital parameter to estimate the thermal-responsive rate of the phase-changeable microcapsules when utilized for regulating the environmental temperature. Figure 12 shows the evolution of thermal conductivities of MEPCMs with increasing loading level of GO-ODA. As compared with the bare MEPCMs (MEPCM00), the increasing percentages of thermal conductivity for MEPCM-01, MEPCM-02 and MEPCM-05 are as high as 9.83 %, 20.29 % and 38.52 %, respectively. When 0.5 % of GO-ODA is involved in the microcapsules, the thermal conductivity reaches to 0.26 W m^{-1} K^{-1}, which is 36.84 % higher than the reported value (0.19 W m^{-1} K^{-1}) for MEPCMs incorporated with 4 % of GO in the shell [18]. Therefore, the incorporation of GO-ODA in the microcapsules could effectively accelerate the thermal transfer, even at a quite limited loading level, and as a result, greatly improve the thermal-responsive capability.

The thermal images of the surface temperature distribution of the bare epoxy disk and the composite disk filled with 20 wt% of MEPCM-05 taken at various times using infrared thermography are illustrated in Fig. 13. It can be seen that, during the initial heating stage from the start to 210 s, the surface temperature of the composite disk increases nearly at the same speed with the epoxy disk without MEPCMs, where the temperature change depends only on the sensible heat [3]. After that, the phase change occurred, the involved *n*-octadecane began to melt and absorb the ambient heat, and the temperature for the composite disk was found to be 5.8 °C, 11.9 °C, 8.6 °C, and 6.2 °C lower than that of the raw epoxy specimen after 270 s, 330 s, 380 s, and 410 s, respectively. The low marked heating effect for the composite specimen suggests that the GO-ODA-filled MEPCMs could effectively suppress the fluctuation of ambient temperature by absorbing/releasing latent heat. When being incorporated into building

materials, textiles and electronic products, etc., the MEPCMs might be conducive for them to realize the targets of energy saving, thermal comfort, and thermal management, respectively. Therefore, they possess a promising application prospect in thermal energy storage and temperature regulation.

4. Conclusions

To substantially improve the compatibility of graphene with the organic core material of MEPCMs and achieve good thermal conductivity without evidently sacrificing the phase-change enthalpy, multi-layered graphene, in this work, were first oxidated using a modified Hummers method and then grafted with octadecylamine to form oleophilic GO-ODA. After that, the GO-ODA-modified MEPCMs were successfully fabricated via in-situ polymerization, in which MF resin was used as the shell material, and the mixture of *n*-octadecane and GO-ODA as the core material. Characterizations of FT-IR, AFM and Raman spectra verified that multi-layered graphene nano-platelets were well exfoliated and alkylated, and have been involved in MEPCMs. Results from FE-SEM observations and laser particle size analysis demonstrated that the size of the as-prepared MEPCMs with a regular spherical shape became smaller when the GO-ODA was incorporated, probably due to the co-emulsion function of GO-ODA during the formation of microcapsules. DSC results revealed that the incorporation of GO-ODA could advance the crystallization process of *n*-octadecane, and thus decrease its supercooling degree in the microcapsule. The MEPCMs exhibited the melting/freezing latent heats as high as 207.2 J g^{-1} and 202.5 J g^{-1}, respectively, and the encapsulation efficiency of higher than 88.0%, which are indicative of a good heat energy-storage capability. Besides, the GO-ODA-incorporated MEPCMs showed a good thermal reliability during the phase change process. The thermal conductivity of the

microcapsules with GO-ODA was greatly enhanced, and with respect to the bare MEPCMs, the increasing percentage of thermal conductivity for MEPCMs containing 0.5 % GO-ODA reached to 38.52 %. Moreover, through the infrared thermography analysis, a lower marked heating effect for the MEPCMs containing GO-ODA was observed during the phase change process of core material. The excellent performances of the GO-ODA-incorporated MEPCMs enable them to be promising for applications in the fields of thermal energy storage and temperature regulation.

Acknowledgements

The authors would like to acknowledge financial supports from the National Natural Science Foundation of China (51173109, 51778369, 51308345), the Guangdong Province Natural Science Foundation of China (2014A030313561) and the Shenzhen Sci & Tech research grant (JCYJ20150625101638041).

References

[1] Su WG, Darkwa J, Kokogiannakis G. Review of solid-liquid phase change materials and their encapsulation technologies. Renew Sust Energ Rev 2015; 48: 373-391.

[2] Zhang Y, Zheng XH, Wang HT, Du QG. Encapsulated phase change materials stabilized by modified graphene oxide. J Mater Chem A 2014; 2: 5304-5314.

[3] Zhang H, Xing F, Cui HZ, Chen DZ, Ouyang X, Xu SZ *et al.* A novel phase-change cement composite for thermal energy storage: Fabrication, thermal and mechanical properties. Appl Energ 2016; 170: 130-139.

[4] Yuan KJ, Wang HC, Liu J, Fang XM, Zhang ZG. Novel slurry containing graphene oxide-grafted microencapsulated phase change material with

enhanced thermo-physical properties and photo-thermal performance. Sol Energ Mat Sol C 2015; 143: 29-37.

[5] Ling ZY, Zhang ZG, Shi GQ, Fang XM, Wang L, Gao XN *et al.* Review on thermal management systems using phase change materials for electronic components, Li-ion batteries and photovoltaic modules. Renew Sust Energ Rev 2014; 31: 427-438.

[6] Makuta T, Kadoya K, Izumi H, Miyatake M. Synthesis of cyanoacrylate-covered xylitol microcapsules for thermal storage. Chem Eng J 2015; 273: 192-196.

[7] Mondal S. Phase change materials for smart textiles - An overview. Appl Therm Eng 2008; 28: 1536-1550.

[8] Zhang W, Ji XQ, Zeng CJ, Chen KL, Yin YJ, Wang CX. A new approach for the preparation of durable and reversible color changing polyester fabrics using thermochromic leuco dye-loaded silica nanocapsules. J Mater Chem C 2017; 5: 8169-8178.

[9] Chen D, Chen Y, Ouyang X, Zuo J, Ye X. Influence of MicroPCMs on thermal and dynamic mechanical properties of a biodegradable P3HB4HB composite. Compos Part B-Eng 2014; 56: 245-248.

[10] Yuan YP, Zhang N, Tao WQ, Cao XL, He YL. Fatty acids as phase change materials: A review. Renew Sust Energ Rev 2014; 29: 482-498.

[11] Dao TD, Jeong HM. A Pickering emulsion route to a stearic acid/graphene core-shell composite phase change material. Carbon 2016; 99: 49-57.

[12] Jiang X, Luo RL, Peng FF, Fang YT, Akiyama T, Wang SF. Synthesis, characterization and thermal properties of paraffin microcapsules modified with nano-Al_2O_3. Appl Energ 2015; 137: 731-737.

[13] Li M, Chen MR, Wu ZS. Enhancement in thermal property and mechanical property of phase change microcapsule with modified carbon nanotube. Appl Energ 2014; 127: 166-171.

[14] Huang Y-T, Zhang H, Wan X-J, Chen D-Z, Chen X-F, Ye X *et al.* Carbon nanotube-enhanced double-walled phase-change microcapsules for thermal energy storage. J Mater Chem A 2017; 5: 7482-7493.

[15] Lee C, Wei XD, Kysar JW, Hone J. Measurement of the elastic properties and intrinsic strength of monolayer graphene. Science 2008; 321: 385-388.

[16] Balandin AA, Ghosh S, Bao WZ, Calizo I, Teweldebrhan D, Miao F *et al.* Superior thermal conductivity of single-layer graphene. Nano Lett 2008; 8: 902-907.

[17] Malas A, Das CK. Effect of graphene oxide on the physical, mechanical and thermo-mechanical properties of neoprene and chlorosulfonated polyethylene vulcanizates. Compos Part B-Eng 2015; 79: 639-648.

[18] Chen ZH, Wang JC, Yu F, Zhang ZG, Gao XN. Preparation and properties of graphene oxide-modified poly(melamine-formaldehyde) microcapsules containing phase change material n-dodecanol for thermal energy storage. J Mater Chem A 2015; 3: 11624-11630.

[19] Yuan K, Wang H, Liu J, Fang X, Zhang Z. Novel slurry containing graphene oxide-grafted microencapsulated phase change material with enhanced thermo-physical properties and photo-thermal performance. Sol Energ Mat Sol C 2015; 143: 29-37.

[20] Hummers WS, Offeman RE. Preparation of Graphitic Oxide. J Am Chem Soc 1958; 80: 1339-1339.

[21] Choudhary S, Mungse HP, Khatri OP. Dispersion of alkylated graphene in organic solvents and its potential for lubrication applications. J Mater Chem A 2012; 22: 21032-21039.

[22] Chen J, Hamon MA, Hu H, Chen YS, Rao AM, Eklund PC *et al.* Solution properties of single-walled carbon nanotubes. Science 1998; 282: 95-98.

[23] Si Y, Samulski ET. Synthesis of water soluble graphene. Nano Lett 2008; 8: 1679-1682.

[24] Lin-Vien D. The Handbook of infrared and raman characteristic frequencies of organic molecules. Boston: Academic Press; 1991.

[25] Niyogi S, Bekyarova E, Itkis ME, McWilliams JL, Hamon MA, Haddon RC. Solution properties of graphite and graphene. J Am Chem Soc 2006; 128: 7720-7721.

[26] Park S, An JH, Jung IW, Piner RD, An SJ, Li XS *et al.* Colloidal suspensions of highly reduced graphene oxide in a wide variety of organic solvents. Nano Lett 2009; 9: 1593-1597.

[27] Gromov A, Dittmer S, Svensson J, Nerushev OA, Perez-Garcia SA, Licea-Jimenez L *et al.* Covalent amino-functionalisation of single-wall carbon nanotubes. J Mater Chem 2005; 15: 3334-3339.

[28] Zhang L, Yang W, Jiang Z, He F, Zhang K, Fan J *et al.* Graphene oxide-modified microencapsulated phase change materials with high encapsulation capacity and enhanced leakage-prevention performance. Appl Energ 2017; 197: 354-363.

[29] Larkin PJ, Makowski MP, Colthup NB, Flood LA. Vibrational analysis of some important group frequencies of melamine derivatives containing

methoxymethyl, and carbamate substituents: mechanical coupling of substituent vibrations with triazine ring modes. Vib Spectrosc 1998; 17: 53-72.

[30] Lu HB, Yao YT, Huang WM, Hui D. Noncovalently functionalized carbon fiber by grafted self-assembled graphene oxide and the synergistic effect on polymeric shape memory nanocomposites. Compos Part B-Eng 2014; 67: 290-295.

[31] Xu XL, Yang CJ, Yang JH, Huang T, Zhang N, Wang Y *et al.* Excellent dielectric properties of poly(vinylidene fluoride) composites based on partially reduced graphene oxide. Compos Part B-Eng 2017; 109: 91-100.

[32] Mensing JP, Wisitsoraat A, Phokharatkul D, Lomas T, Tuantranont A. Novel surfactant-stabilized graphene-polyaniline composite nanofiber for supercapacitor applications. Compos Part B-Eng 2015; 77: 93-99.

[33] Tuinstra F, Koenig JL. Raman spectrum of graphite. J Chem Phys 1970; 53: 1126.

[34] Oliver MJ, Calvert PD. Homogeneous nucleation of *n*-alkanes measured by differential scanning calorimetry. J Cryst Growth 1975; 30: 343-351.

[35] Zhang XX, Fan YF, Tao XM, Yick KL. Crystallization and prevention of supercooling of microencapsulated *n*-alkanes. J Colloid Interf Sci 2005; 281: 299-306.

[36] Zhu YL, Liang S, Chen KP, Gao X, Chang PP, Tian CR *et al.* Preparation and properties of nanoencapsulated n-octadecane phase change material with organosilica shell for thermal energy storage. Energ Convers Manage 2015; 105: 908-917.

Figure legends

Fig. 1. Schematic modification of NGP.

Fig. 2. Schematic synthesis of GO-ODA-filled MEPCMs.

Fig. 3. FTIR spectra of GO, ODA and GO-ODA. The inset shows the dispersion of GO-ODA in (a) melted *n*-octadecane and (b) deionized water for 24 h.

Fig. 4. AFM images and height profiles of (a, c) GO and (b, d) GO-ODA.

Fig 5. The color of MEPCM powders. (a) MEPCM-00, (b) MEPCM-05.

Fig. 6. FE-SEM images of (a) MEPCM-00, (b) MEPCM-01, (c) MEPCM-02, (d) MEPCM-05 and (e) a fractured microcapsule, and (f) the particle size distributions of MEPCMs.

Fig. 7. FTIR spectra of GO-ODA, MF resin, n-octadecane, MEPCM-00 and MEPCM-01.

Fig. 8. Raman spectra of GO-ODA, MEPCM-00, MEPCM-01, MEPCM-02, and MEPCM-05.

Fig. 9. XRD patterns of GO-ODA, MF resin, *n*-octadecane, MEPCM-00 and MEPCM-01.

Fig. 10. DSC curves of *n*-octadecane and MEPCMs. (a) Melting process; (b) freezing process

Fig. 11. Thermal conductivities and their increasing percentages of MEPCMs with and without GO-ODA.

Fig. 12. DSC curves of (a) MEPCM-00 and (b) MEPCM-05 after experiencing 1, 10, 20 and 30 heating-cooling cycles.

Fig.13. Infrared thermography images of the round disks of pure epoxy resin and the MEPCM05-filled composite after heated for different periods.

Fig. 1

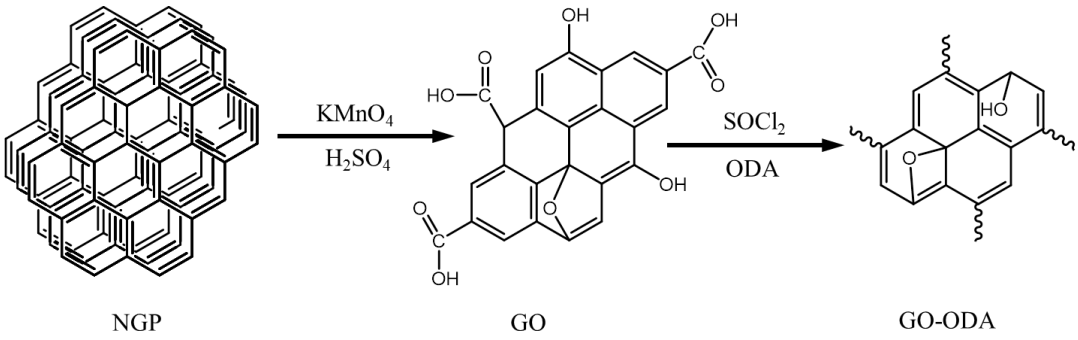
KMnO4
H2SO4
SOCl2
ODA
NGP
GO
GO-ODA

Fig. 2

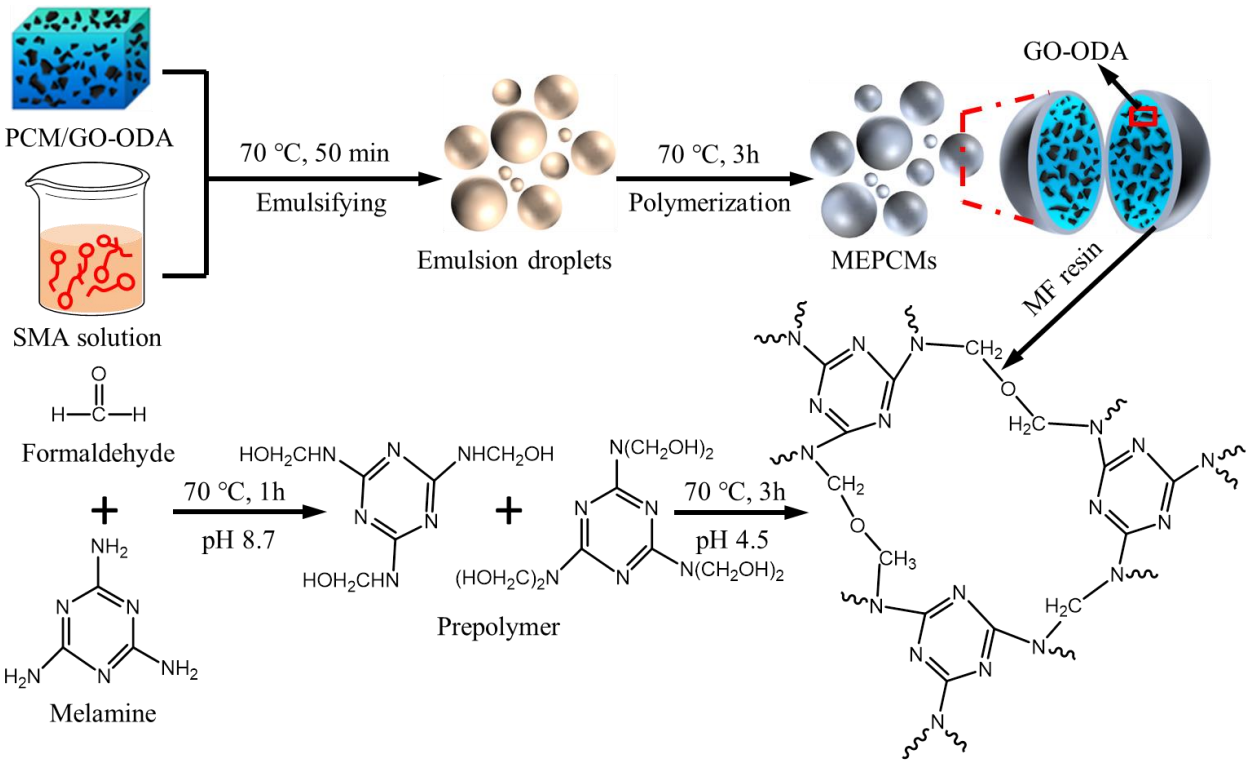
PCM/GO-ODA
SMA solution
70 °C, 50 min
Emulsifying
Emulsion droplets
70 °C, 3h
Polymerization
MEPCMs
GO-ODA
MF resin
Formaldehyde
70 °C, 1h
pH 8.7
Prepolymer
70 °C, 3h
pH 4.5
Melamine

Fig. 3

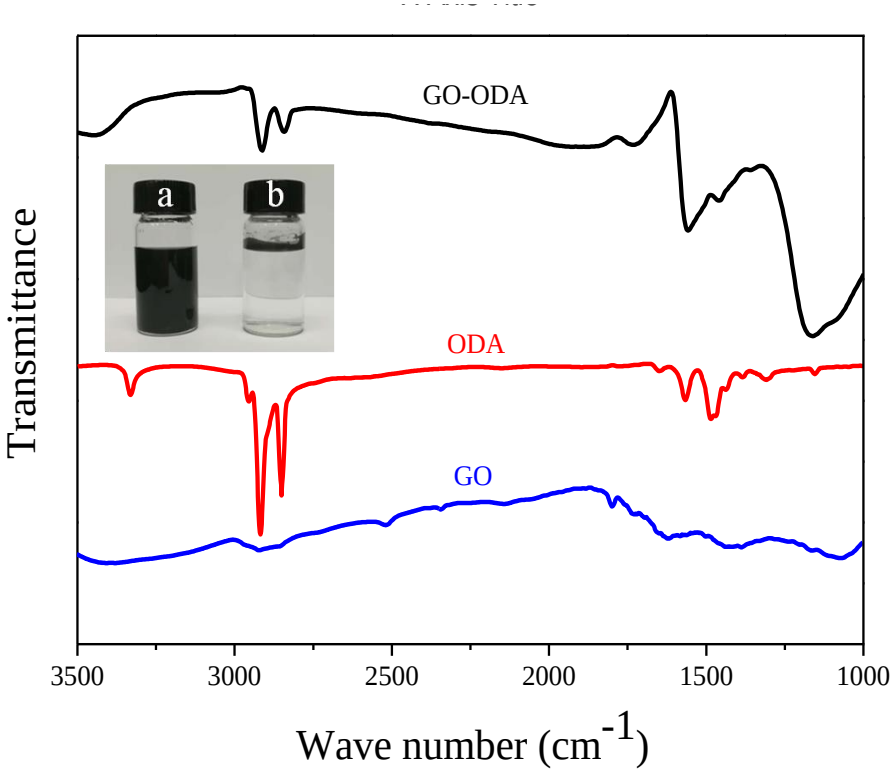
GO-ODA
a
b
ODA
GO
Transmittance
3500
3000
2500
2000
1500
1000
Wave number (cm-1)

Fig. 4

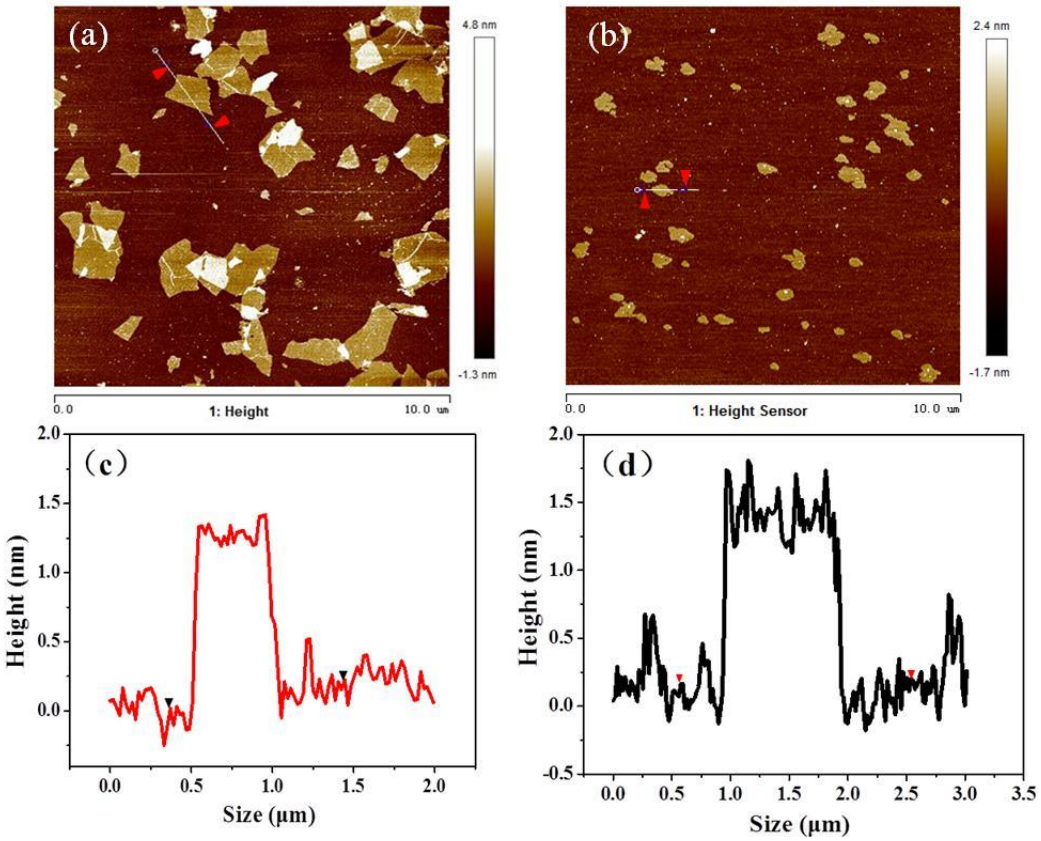
(a)
4.8 nm
-1.3 nm
0.0
1: Height
10.0 um
(b)
2.4 nm
-1.7 nm
0.0
1: Height Sensor
10.0 um
(c)
Height (nm)
Size (μm)
(d)
Height (nm)
Size (μm)

Fig. 5

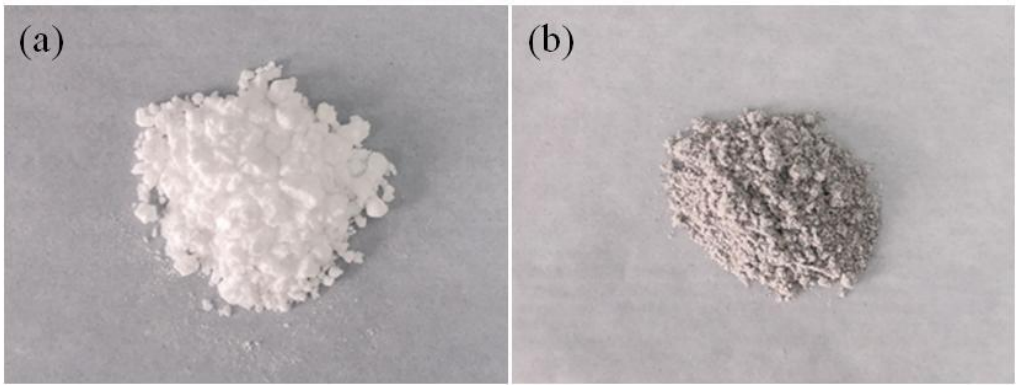
(a)
(b)

Fig. 6

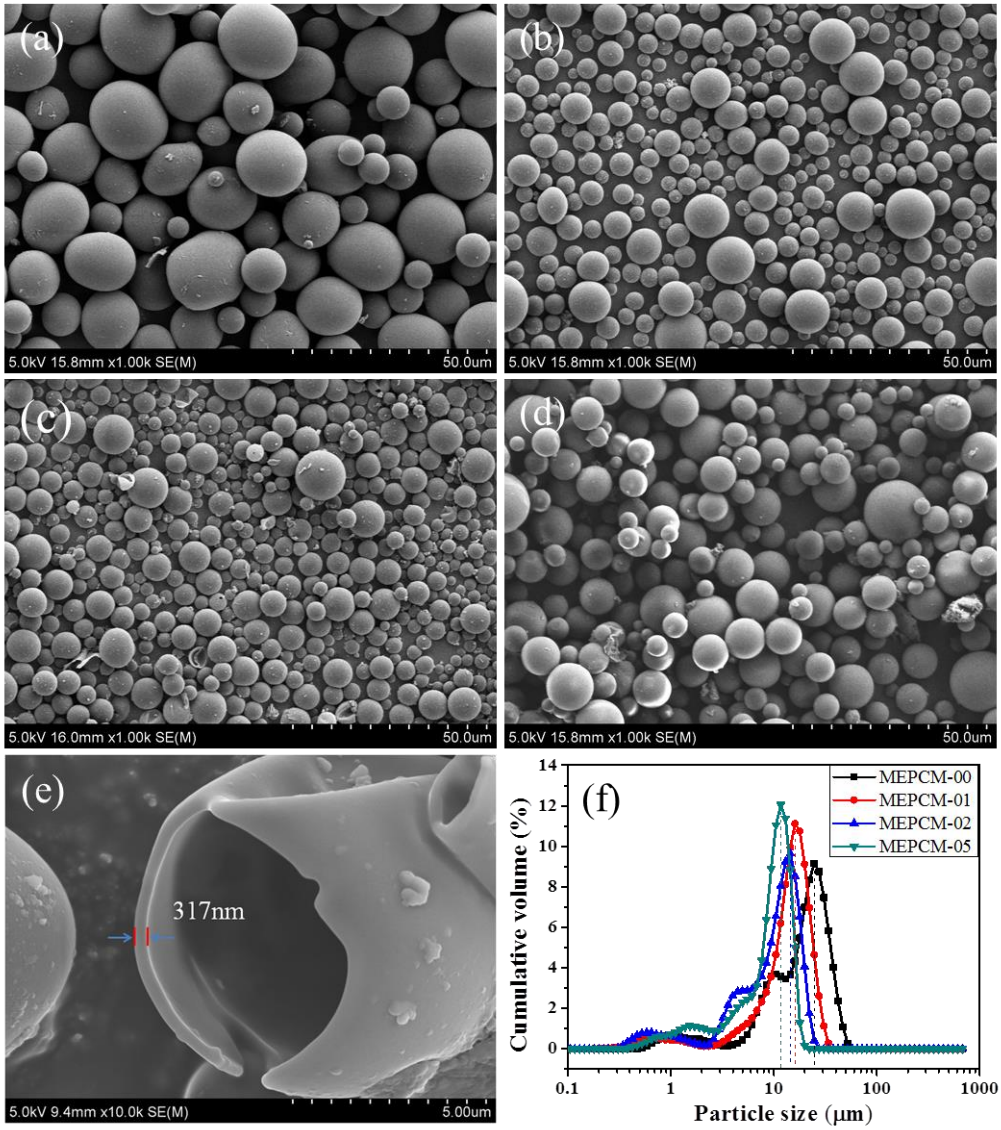
(a)
5.0kV 15.8mm x1.00k SE(M)
50.0um
(b)
5.0kV 15.8mm x1.00k SE(M)
50.0um
(c)
5.0kV 16.0mm x1.00k SE(M)
50.0um
(d)
5.0kV 15.8mm x1.00k SE(M)
50.0um
(e)
317nm
5.0kV 9.4mm x10.0k SE(M)
5.00um
(f)
MEPCM-00
MEPCM-01
MEPCM-02
MEPCM-05
Cumulative volume (%)
Particle size (μm)
0
2
4
6
8
10
12
14
0.1
1
10
100
1000

Fig. 7

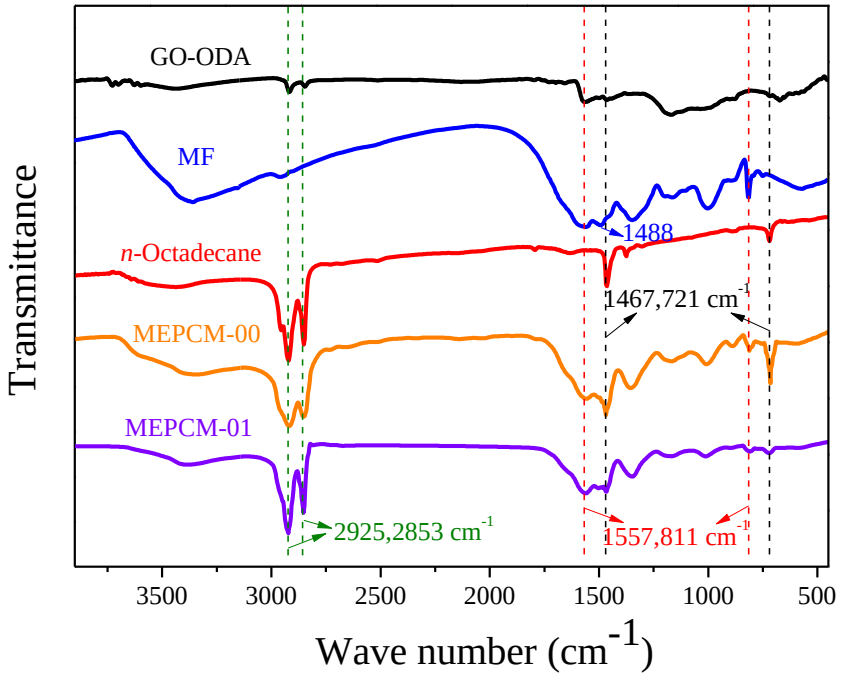
GO-ODA
MF
1488
n-Octadecane
1467,721 cm-1
MEPCM-00
MEPCM-01
2925,2853 cm-1
1557,811 cm-1
Transmittance
3500
3000
2500
2000
1500
1000
500
Wave number (cm-1)

Fig. 8

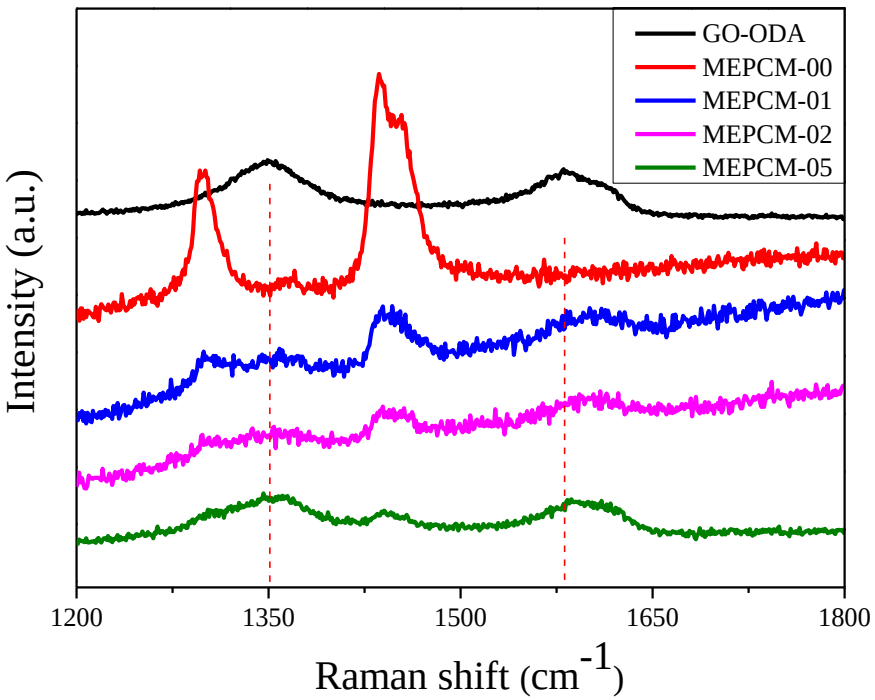
GO-ODA
MEPCM-00
MEPCM-01
MEPCM-02
MEPCM-05
Intensity (a.u.)
1200
1350
1500
1650
1800
Raman shift (cm-1)

Fig. 9

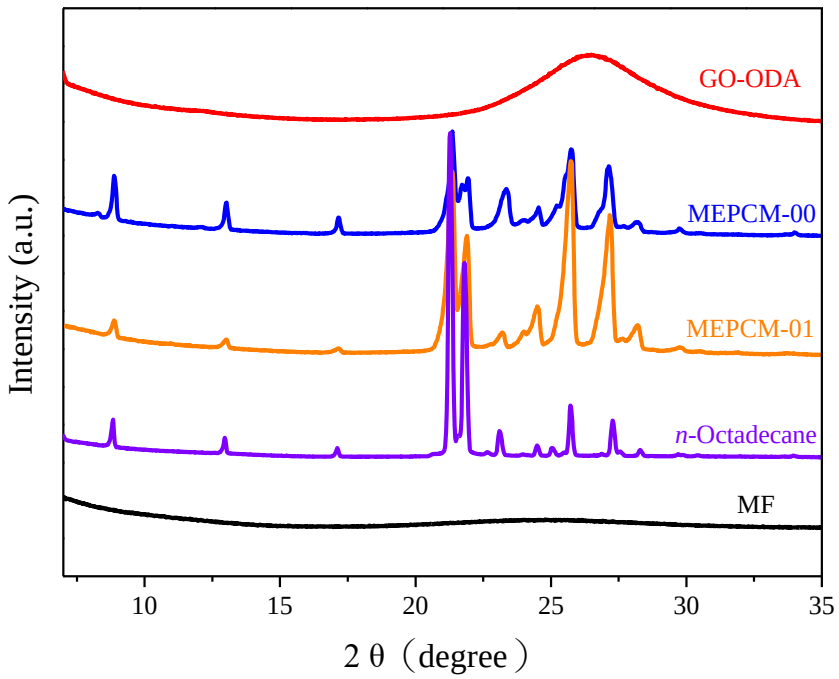
GO-ODA
MEPCM-00
MEPCM-01
n-Octadecane
MF
Intensity (a.u.)
10
15
20
25
30
35
2 θ（degree）

Fig. 10

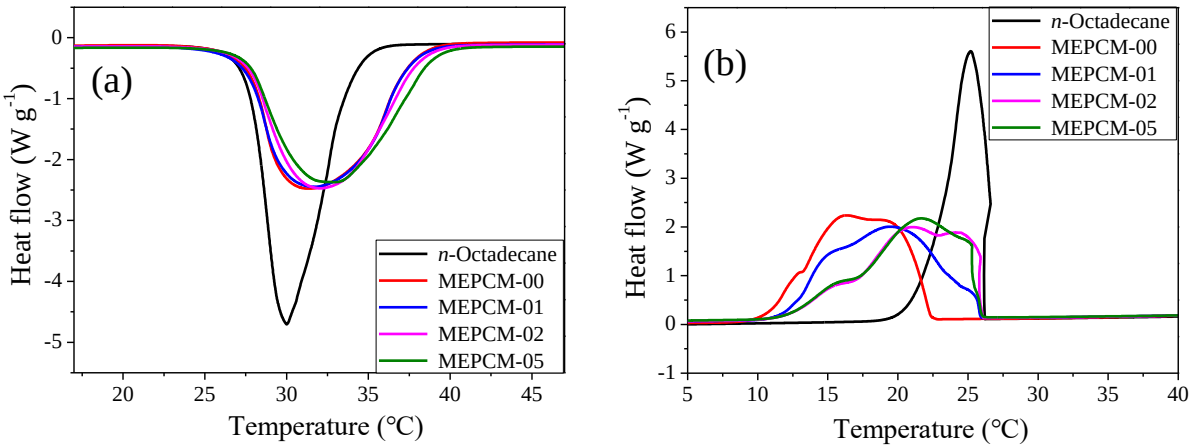
(a)
Heat flow (W g-1)
Temperature (°C)
n-Octadecane
MEPCM-00
MEPCM-01
MEPCM-02
MEPCM-05
(b)
Heat flow (W g-1)
Temperature (°C)
n-Octadecane
MEPCM-00
MEPCM-01
MEPCM-02
MEPCM-05

Fig. 11

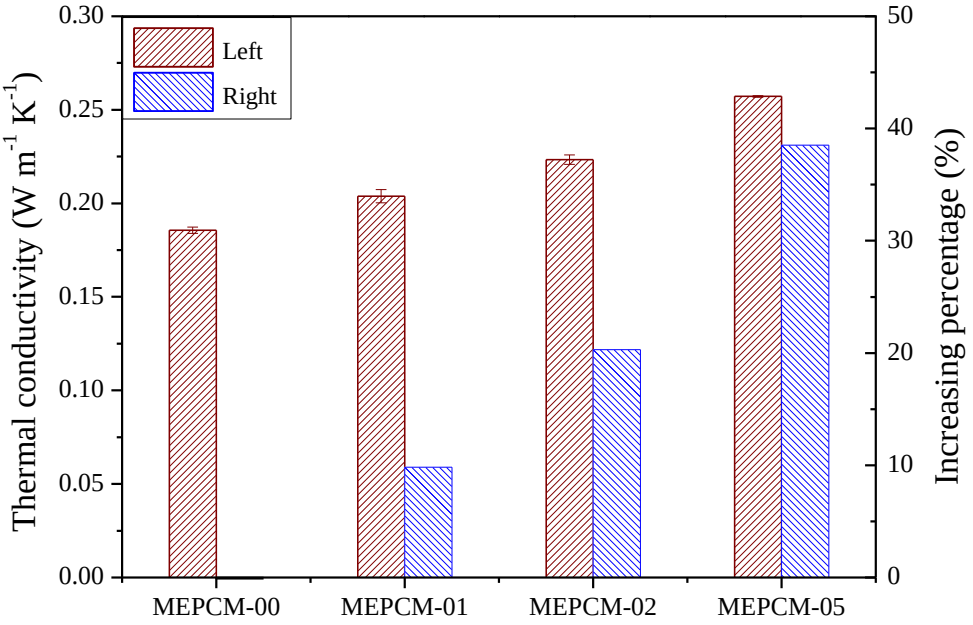
Left
Right
Thermal conductivity (W m-1 K-1)
Increasing percentage (%)
0.00
0.05
0.10
0.15
0.20
0.25
0.30
0
10
20
30
40
50
MEPCM-00
MEPCM-01
MEPCM-02
MEPCM-05

Fig. 12

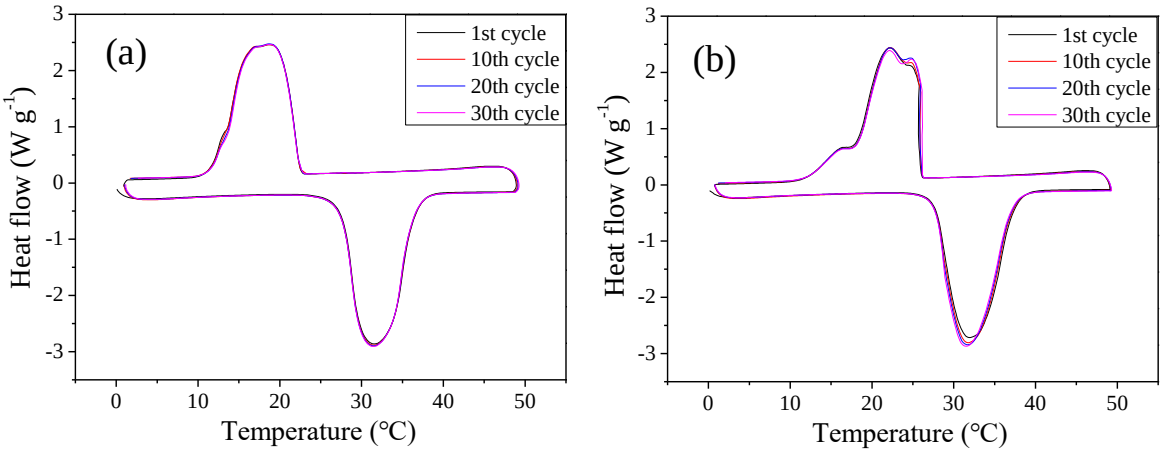
(a)
(b)
1st cycle
10th cycle
20th cycle
30th cycle
Heat flow (W g-1)
Temperature (°C)

.

Fig. 13

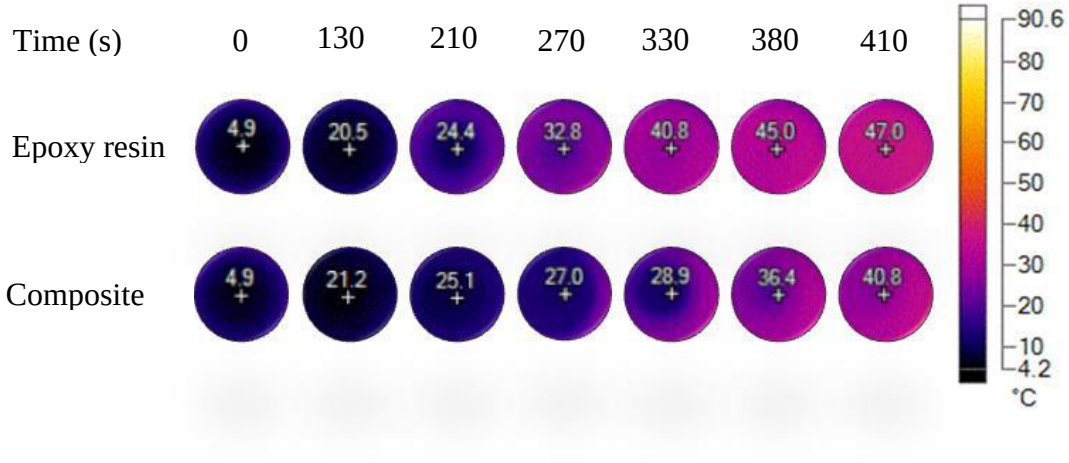
Time (s)
0
130
210
270
330
380
410
Epoxy resin
4.9
20.5
24.4
32.8
40.8
45.0
47.0
Composite
4.9
21.2
25.1
27.0
28.9
36.4
40.8
90.6
80
70
60
50
40
30
20
10
4.2
°C

Tables

Table 1 The prescriptions of MEPCMs with and without GO-ODA.

.

Reagents	Weight (g)			
	MEPCM-00	MEPCM-01	MEPCM-02	MEPCM-05
n-Octadecane	25	25	25	25
5% SMA	30	30	30	30
Distilled water	20	20	20	20
Melamine	6	6	6	6
Formaldehyde	11	11	11	11
GO-ODA	0	0.025	0.050	0.125

Table 2 Thermal properties of *n*-octadecane and MEPCMs.

Samples	Melting process					Freezing process					*E* [%]
	$T_{m,s}$ [℃]	T_m [℃]	$T_{m,e}$ [℃]	$\Delta T_{m,w}$ [℃]	ΔH_m [J g^{-1}]	$T_{f,s}$ [℃]	T_α [℃]	T_β [℃]	T_γ [℃]	ΔH_f [J g^{-1}]	
n-Octadecane	27.38	30.00	33.96	6.58	233.1	26.20	-	25.17	-	232.5	100
MEPCM-00	27.47	31.41	37.78	10.31	218.1	22.51	19.33	16.26	12.88	214.2	92.8
MEPCM-01	27.48	31.71	37.68	10.02	214.5	25.90	25.22	19.44	15.51	210.9	91.3
MEPCM-02	27.43	32.08	38.32	10.89	210.2	26.03	24.56	20.98	16.05	205.8	89.3
MEPCM-05	27.51	32.93	39.01	11.50	207.2	26.04	25.07	21.64	16.05	202.5	88.0